

Hall effect test bench for temperature dependence of carrier concentration

Abstract. This paper presents an integrated bench for Hall effect measurements consisting of a helium cryostat placed between the electromagnet poles with a field of 0.5 T and a control and measurement system, as well as control algorithm for different operating modes. The results of measurements of majority carrier concentration by van der Pauw method in the temperature range 165 K - 300 K for indium tin oxide (ITO).

Streszczenie. W artykule przedstawiono zintegrowane stanowisko do pomiaru efektu Hall'a składające się z helowego kriostatu umieszczonego między nabiegownikami elektromagnesu o polu 0,5 T oraz systemu kontrolno-pomiarowego, a także algorytmu sterowania dla różnych trybów pracy. Zaprezentowano wyniki pomiarów koncentracji nośników większościowych metodą van der Pauw'a w zakresie temperatur od 165 K do 300 K dla warstw tlenku indowo-cynowego (ITO). (Stanowisko do pomiarów efektu Hall'a do wyznaczania temperaturowych zależności koncentracji nośników).

Keywords: Hall effect, van der Pauw method, carrier concentration, thin films

Słowa kluczowe: efekt Halla, metoda van der Pauw, koncentracja nośników, cienkie warstwy

Introduction

Electrical conductivity of materials is determined by the carrier concentration, mobility and also sign of carrier. For this reason, measurements of these parameters are important for studying the properties of materials used in electronics. The knowledge of concentration and mobility of carriers at different temperatures, including cryogenic temperatures, is particularly important due to the growing interest in low temperature applications of microelectronic devices [1][2][3][4]. One of the best known methods for measuring these parameters is based on the Hall effect, in which the Hall voltage V_H is measured [5][6]. Hall voltage is described by equation (1):

$$(1) \quad V_H = \frac{IB}{qn}$$

where I is the current, B is the magnetic field, q is the elementary charge and n is the charge carrier density [7].

The phenomenon of voltage generation under the influence of current flow and an applied magnetic field was discovered in 1879 by physicist Edwin Hall and called his name.

The Hall effect is the basis for many devices. Hall effect sensors are used for example in current sensing [7], variable speed drives [8], motor control protection/indicators, motion sensing [9], diaphragm pressure gage [10], flow meters [11], direct current electricity [12] and rotational speed sensor [13]. Hall sensors are used in medical applications such as detecting DNA [14], monitoring pulse wave velocity of blood [15], characterizing soft biological materials [16][17], etc.

One of the methods of determining the electrical conductivity, the resistivity, the Hall constant, the charge carrier concentration and the charge carrier mobility is the van der Pauw method [18]. The diagram of the electrodes in the van der Pauw configuration is shown in Figure 1.

The resistivity ρ of a material of known thickness d is calculated from the following formula (2):

$$(2) \quad \rho = R_S \cdot d$$

where R_S is sheet resistance.

In order to determine the resistivity it is necessary to determine the values of sheet resistance R_S which can be

calculated numerically from the equation (3):

$$(3) \quad \exp\left(\frac{\pi R_A}{R_S}\right) + \exp\left(\frac{\pi R_B}{R_S}\right) = 1$$

where R_A and R_B are the characteristic resistances. Resistances R_A and R_B and can be determined from the following equations (4) and (5):

$$(4) \quad R_A = \frac{R_{21,34} + R_{12,43} + R_{43,12} + R_{34,21}}{4}$$

$$(5) \quad R_B = \frac{R_{32,41} + R_{23,14} + R_{14,23} + R_{41,32}}{4}$$

where: $R_{12,43}$ is the resistance calculated for the current I_{12} , injected into pin 2 and drawn from pin 1 and the voltage V_{43} measured between pins 4 and 3.

An analogous procedure is followed to determine the other resistances: $R_{21,34}$, $R_{43,12}$, $R_{34,21}$, $R_{32,41}$, $R_{23,14}$, $R_{14,32}$, $R_{41,32}$.

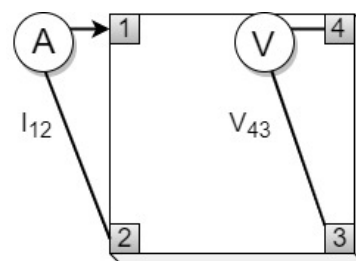


Fig. 1. Experimental setup for Van-der-Pauw measurement

Determination of concentration and mobility of current carriers as well as type of conductivity (n or p) is possible by measuring voltages and applied currents in the presence of magnetic field induction B . In order to eliminate measurement errors resulting, for example, from asymmetrical contact placement, two sets of measurements are performed for positive (S) and negative (N) magnetic field directions. To determine the concentration of current carrier n_s , it is necessary to know the value of the direct current I_{13} injected into pin 1 and drawn from pin 3 and to measure the Hall voltage V_{24P} in the positive magnetic field. A similar measurement procedure is performed to measure

the Hall voltage for the other pins: V_{42S} , V_{13S} and V_{31S} for currents I_{13} , I_{31} , I_{42} and I_{24} , respectively. Analogous measurements are made for the negative magnetic field to measure the Hall voltage of V_{42N} , V_{13N} and V_{31N} for currents I_{13} , I_{31} , I_{42} and I_{24} respectively. Knowing the values of Hall voltages, the sheet carrier density can be calculated from equation (6):

$$(6) \quad n_s = 8 \cdot 10^{-8} \frac{I \cdot B}{q \cdot |V_i|}$$

where $|V_i| = V_C + V_D + V_E + V_F$ is the sum of measured Hall voltages including their signs, while $V_C = V_{24S} - V_{24N}$, $V_D = V_{42S} - V_{42N}$, $V_E = V_{13S} - V_{13N}$, $V_F = V_{31S} - V_{31N}$ (in voltage V), B is magnetic field induction in gauss [G], I is the dc current in amperes [A] and q is the elementary charge ($1.602 \cdot 10^{-19}$ C). Also, the bulk carrier density n [cm^{-3}] can be determined by knowing the thickness d of the sample:

$$(7) \quad n = \frac{n_s}{d}$$

Knowing the concentration of current carriers n_s and sheet resistance R_s from resistivity measurements ρ , it is possible to calculate the mobility of current carriers μ by the formula:

$$(8) \quad \mu = \frac{1}{q \cdot n_s \cdot R_s}$$

Many Hall measurement results are focused on the changes in mobility, charge concentration, resistivity and type of conductivity of the layers under the influence of temperature change and doping etc. The use of different methods to obtain semiconductor materials also causes differences in their structure and properties. An example can be zinc oxide (ZnO), which obtained by two different methods, i.e., chemical vapor deposition and hydrothermal method, is characterized by different carrier concentration [19]. The highest mobility of current carriers (electrons) $166 \text{ cm}^2/\text{Vs}$ was obtained for the layers obtained by hydrothermal method with a carrier concentration of $1.65 \times 10^{17} \text{ cm}^{-3}$. Hall effect measurements also showed that the growth temperature of the layers plays a key role in determining the type of conductivity. The results for nitrogen-doped ZnO layers were prepared by metalorganic chemical vapour deposition (MOCVD) [20]. The results show that p-type resistivity can be achieved at all growth temperatures except $500 \text{ }^\circ\text{C}$. The layer obtained at $400 \text{ }^\circ\text{C}$ is characterized by a resistivity of $1.72 \text{ } \Omega\text{cm}$, a mobility of $1.59 \text{ cm}^2/\text{Vs}$, and a hole concentration of $2.29 \times 10^{18} \text{ cm}^{-3}$. The temperature increase above $450 \text{ }^\circ\text{C}$ reduces the incorporation of nitrogen (acceptor dopant) in ZnO thin films, which may account for the relatively low hole concentration of $3.68 \times 10^{16} \text{ cm}^{-3}$ or even the change in conductivity to n-type [20][21][22]. Tampo et al [23] prepared ZnMgO/ZnO/MgO metal oxide heterostructure on sapphire substrate using molecular beam epitaxy (MBE) method. This resulted in a high electron mobility of $250 \text{ cm}^2/\text{Vs}$ and a low carrier concentration of $1 \times 10^{13} \text{ cm}^{-2}$ at room temperature (RT). The change of electrical properties of ZnO layers is also carried out by Zr doping. The results of the layers obtained by ALD method, whose electrical properties were determined by four-point probe (4PP) and Hall effect measurements [24]. The carrier concentration increases from 1.0×10^{20} to $3.81 \times 10^{20} \text{ cm}^{-3}$ as the doping increases from zero to 4.8 at.%, leading to a decrease in resistivity from 3.02×10^{-3} to $1.44 \times 10^{-3} \text{ } \Omega\text{cm}$. In addition, the effect of annealing the CuO layers on the electrical properties was investigated [24]. The CuO layers showed n-

type resistivity after annealing at $100 \text{ }^\circ\text{C}$. The resistivity changed to p-type for the layers annealed at 200 to $300 \text{ }^\circ\text{C}$, in which the Cu_2O phase was dominant. However, the resistivity reverted to n-type for further increase in annealing temperature up to $350 \text{ }^\circ\text{C}$, where CuO phase dominates [24]. Also, the mobility and concentration of carriers in WO_3 were determined [25]. The electron mobility in the 5 nm thick layer was $560 \text{ cm}^2/\text{Vs}$ and decreased to $10 \text{ cm}^2/\text{Vs}$ for thicker layers above 30 nm .

This paper presents an integrated Hall effect test bench consisting of a helium cryostat placed between the poles of electromagnet with a field of 0.5 T and a control and measurement system, as well as control algorithms for different operating modes. The results of test measurements of majority carrier concentration by van der Pauw method in the temperature range 165 K - 300 K for 100 nm thick indium tin oxide (ITO) layers are presented.

System description

The presented Hall-effect measurement system is a part of the Laboratory of Vacuum and Thin Film Technologies in the Institute of Electronics, AGH University of Science and Technology. The Hall measurement system with the laboratory equipment components is shown in Figure 1 and Figure 2.



Fig. 2. Low temperature cryostat with control unit

The test system consists of four parts:

- vacuum system,
- helium optical cryostat,
- electromagnet,
- control unit.

The electromagnet capable of generating magnetic field induction of up to 0.5 T . The electromagnet coils are cooled by a constant flow of water. The helium cryostat and in particular its cryogenic part, the cold finger, is located between the electromagnet poles. The chamber containing the cold finger is pumped to a pressure of min. 10^{-3} hPa . The cold finger is equipped with a PT100 temperature sensor, a resistance heater and a substrate holder. The cold finger can be cooled by pumping liquid nitrogen vapor or flooding the chamber with liquid nitrogen.

Hall measurements can be performed using the van der Pauw, 6-point and classical Greek-cross methods. The signals are routed out through thin wires in cotton lagging to a signal head located outside the cryostat. The pumping set, pressure set and measuring head are connected by a control and measurement system.

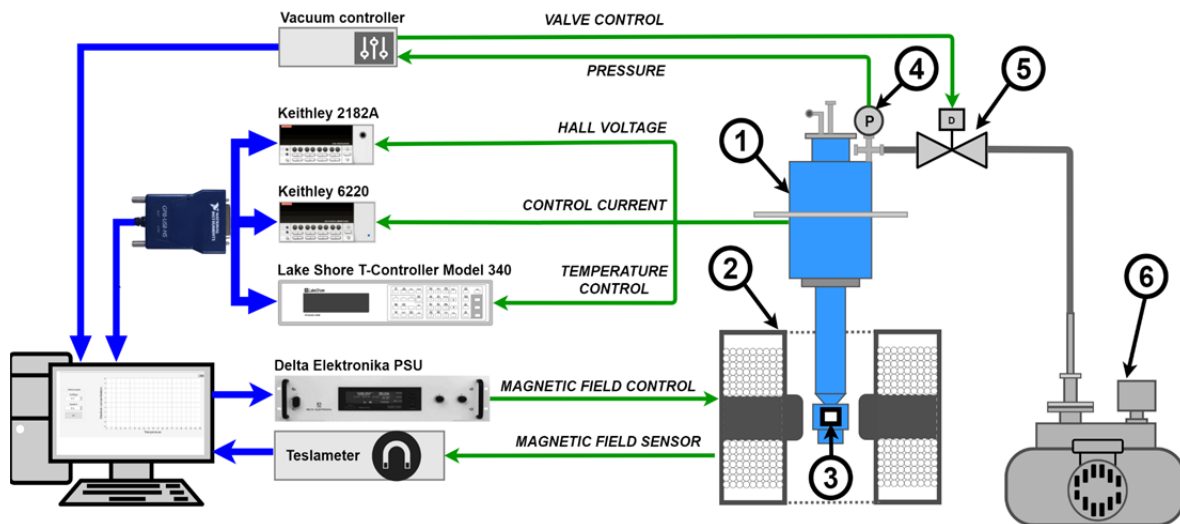


Fig. 3. Laboratory measurement equipment for Hall effect investigation. Markings in the figure: (1) cryostat, (2) magnetic field of the electromagnet, (3) tested sample, (4) pressure sensor, (5) shut-off valve and (6) vacuum pump

Control and measurement system

The scheme of the control and measurement system prepared for the experiments is shown in Figure 3. Stable measuring conditions in the cryostat (1) that keeps the tested sample (3) in the magnetic field of the electromagnet (2) are provided by the vacuum controller. It monitors the operation of the vacuum pump (6) on the basis of the signal from the pressure sensor (4) manufactured by INFICON, and when the appropriate conditions are reached, it switches off the pump and closes the shut-off valve (5). The electromagnetic field is controlled in the software by a magnetic field control system consisting of a field measuring system (Teslometer + CYSJ362A sensor) and a Delta Elektronik power supply. The temperature of the sample is controlled by a Lake Shore 340 temperature control system working with a PT1000 sensor and a miniature resistance heater mounted in the substrate holding the sample in the cryostat. The current excitation and Hall voltage are measured by a Keithley 6220 current source assembly and a Keithley 2182A nanovoltmeter, respectively.

The test bench operates under the control of the program executed in LabVIEW programming environment by National Instruments. The program was implemented as a multi-threaded control and measurement application allowing for monitoring of the test stand and real-time sample measurements.

Measurements

The system was tested by investigating the electrical properties of 100 nm thick ITO layers over a wide temperature range from 165 K to 350 K. The studies confirm that ITO is an n-type semiconductor and is characterized by low electrical resistivity of 10^{-4} Ω .cm. Electrical resistivity and carrier concentration dependence on temperature for ITO thin film is presented in Figure 4.

Conclusions

This paper presents a description of a system constructed at the Institute of Electronics to study the concentration of current carriers by Hall measurements. The results of test measurements of ITO layers in the temperature range 165 K - 300 K are presented. The results

obtained are in good agreement with literature data [26][27]. The measurement system can operate in manual mode as well as in automatic mode, where the algorithm allows for the determination of characteristics such as concentration and mobility of carriers, resistance, resistivity, conductivity and Hall constant as a function of temperature.

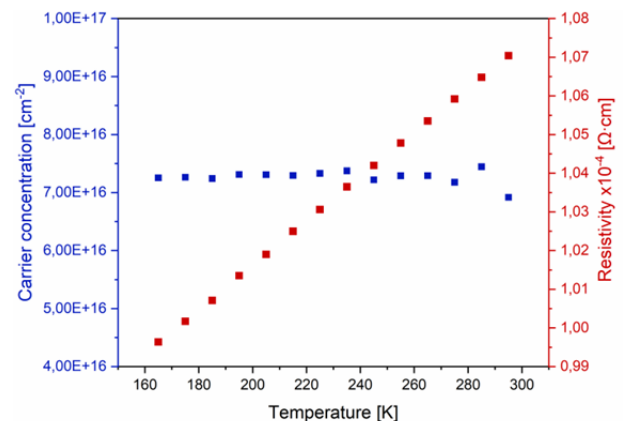


Fig. 4. Electrical resistivity and carrier concentration dependence on temperature for ITO thin film

Acknowledgments

The paper was financially supported by Institute of Electronic AGH project no 16.16.230.434.

Authors: dr inż. Katarzyna Dyndał, AGH University of Science and Technology, Institute of Electronics, Al. Mickiewicza 30, Kraków, Poland, E-mail: kkoper@agh.edu.pl; dr. inż. Zbigniew Sobków, Hasler Rail, IBU On-Board Electronics, Podnikatelská 556, Praha, Czech Republic, email: Zbigniew.Sobkow@haslerrail.com; prof. dr hab. Jerzy Sanetra, The author is retired, pusanetr@cyf-kr.edu.pl; dr hab. inż., prof AGH Konstancy W. Marszałek, AGH University of Science and Technology, Institute of Electronics, Al. Mickiewicza 30, Kraków, Poland, E-mail: marszalek@agh.edu.pl

REFERENCES

- [1] H. Gui *et al.*, "Review of Power Electronics Components at Cryogenic Temperatures," *IEEE Trans Power Electron.*, vol. 35, no. 5, pp. 5144–5156, 2021, doi: 10.1109/tpe.2019.2944781.Review.
- [2] J. Jankowski, S. El-Ahmar, and M. Oszwaldowski, "Hall sensors for extreme temperatures," *Sensors*, vol. 11, no. 1, pp. 876–885, 2011, doi: 10.3390/s110100876.

- [3] I. Tobehn-Steinhäuser, M. Reiche, M. Schmelz, R. Stolz, T. Fröhlich, and T. Ortlepp, "Carrier Mobility in Semiconductors at Very Low Temperatures," *Eng. Proc.*, vol. 6, pp. 1–5, 2021, doi: 10.3390/i3s2021dresden-10086.
- [4] G. Wroblewski *et al.*, "Graphene platelets as morphology tailoring additive in carbon nanotube transparent and flexible electrodes for heating applications," *J. Nanomater.*, vol. 2015, 2015, doi: 10.1155/2015/316315.
- [5] E. H. Hall, "On a New Action of the Magnet on Electric Currents," *Am. J. Math.*, vol. 2, pp. 287–292, 1879.
- [6] G. S. Leadstone, "The discovery of the Hall effect," *Phys. Educ.*, vol. 14, no. 6, pp. 374–379, 1979, doi: 10.1088/0031-9120/14/6/001.
- [7] N. H. C. Techniques, "Product Information Provide Safe , Reliable Detection and Protection for Power Electronics," no. 1, pp. 1–19.
- [8] W. P. N. dos Reis, G. E. Couto, and O. Morandin Junior, "Direct current geared motor data: Voltage, current, and speed measured under different experimental conditions," *Data Br.*, vol. 40, p. 107802, 2022, doi: 10.1016/j.dib.2022.107802.
- [9] R. Garmabdari, S. Shafie, W. Z. Wan Hassan, and A. Garmabdari, "Study on the effectiveness of dual complementary Hall-effect sensors in water flow measurement for reducing magnetic disturbance," *Flow Meas. Instrum.*, vol. 45, pp. 280–287, 2015, doi: 10.1016/j.flowmeasinst.2015.07.007.
- [10] S. Paliwal and S. Yenuganti, "A Differential Hall Effect Based Pressure Sensor," *J. Electr. Eng. Technol.*, vol. 16, no. 2, pp. 1119–1129, 2021, doi: 10.1007/s42835-020-00647-8.
- [11] M. Urbański, M. Nowicki, R. Szewczyk, and W. Winiarski, "Flowmeter Converter Based on Hall Effect Sensor," *Adv. Intell. Syst. Comput.*, vol. 352, pp. 265–276, 2015, doi: 10.1007/978-3-319-15835-8_29.
- [12] S. D. T. Dewi, C. Panatarani, and I. M. Joni, "Design and development of DC high current sensor using Hall-Effect method," *AIP Conf. Proc.*, vol. 1712, no. February 2016, pp. 1–6, 2016, doi: 10.1063/1.4941871.
- [13] C. Liu, J. G. Liu, and R. Kennel, "Accuracy Improvement of Rotational Speed Sensors by Novel Signal Processing Method," *J. Phys. Conf. Ser.*, vol. 1065, no. 7, pp. 0–4, 2018, doi: 10.1088/1742-6596/1065/7/072013.
- [14] S. M. Hira *et al.*, "Detection of Target ssDNA Using a Microfabricated Hall Magnetometer with Correlated Optical Readout," *J. Biomed. Biotechnol.*, pp. 1–10, 2012, doi: 10.1155/2012/492730.
- [15] P. M. Nabeel, J. Joseph, and M. Sivaprakasam, "A Magnetic Plethysmograph Probe for Local Pulse Wave Velocity Measurement," *IEEE Trans. Biomed. Circuits Syst.*, vol. 11, no. 5, pp. 1065–1076, 2017, doi: 10.1109/TBCAS.2017.2733622.
- [16] D. E. Backman, B. L. LeSavage, and J. Y. Wong, "Versatile and inexpensive Hall-Effect force sensor for mechanical characterization of soft biological materials," *J. Biomech.*, vol. 51, pp. 118–122, 2017, doi: 10.1016/j.jbiomech.2016.11.065.
- [17] H. Fan *et al.*, "Detection techniques of biological and chemical Hall sensors," *RSC Adv.*, vol. 11, no. 13, pp. 7257–7270, 2021, doi: 10.1039/d0ra10027g.
- [18] F. S. Oliveira, R. B. Cipriano, F. T. da Silva, E. C. Romão, and C. A. M. dos Santos, "Simple analytical method for determining electrical resistivity and sheet resistance using the van der Pauw procedure," *Sci. Rep.*, vol. 10, no. 1, pp. 1–8, 2020, doi: 10.1038/s41598-020-72097-1.
- [19] N. A. Jayah, H. Yahaya, M. R. Mahmood, T. Terasako, K. Yasui, and A. M. Hashim, "High electron mobility and low carrier concentration of hydrothermally grown ZnO thin films on seeded a-plane sapphire at low temperature," *Nanoscale Res. Lett.*, vol. 10, no. 1, pp. 1–10, 2015, doi: 10.1186/s11671-014-0715-0.
- [20] Y. J. Zeng *et al.*, "Study on the Hall-effect and photoluminescence of N-doped p-type ZnO thin films," *Mater. Lett.*, vol. 61, pp. 41–44, 2007, doi: 10.1016/j.matlet.2006.04.001.
- [21] A. Tsukazaki *et al.*, "Systematic examination of carrier polarity in composition spread ZnO thin films codoped with Ga and N," *Appl. Phys. Lett.*, vol. 81, pp. 235–237, 2002, doi: 10.1063/1.1491294.
- [22] M. Sumiya *et al.*, "Quantitative control and detection of heterovalent impurities in ZnO thin films grown by pulsed laser deposition," *J. Appl. Phys.*, vol. 93, pp. 2562–2569, 2003, doi: 10.1063/1.1542938.
- [23] H. Tampo *et al.*, "High electron mobility Zn polar ZnMgO/ZnO heterostructures grown by molecular beam epitaxy," *J. Cryst. Growth*, vol. 301–302, pp. 358–361, 2007, doi: 10.1016/j.jcrysgro.2006.11.169.
- [24] S. Herodotou, R. E. Treharne, K. Durose, G. J. Tatlock, and R. J. Potter, "The effects of Zr doping on the optical, electrical and microstructural properties of thin ZnO films deposited by atomic layer deposition," *Materials (Basel)*, vol. 8, pp. 7230–7240, 2015, doi: 10.3390/ma8105369.
- [25] H. Mito *et al.*, "High-Mobility Single-Crystalline WO₃ Epitaxial Films Grown on LSAT Substrates," *IMFEDK 2018 - 2018 Int. Meet. Futur. Electron Devices, Kansai*, vol. 2018, pp. 3–4, 2018, doi: 10.1109/IMFEDK.2018.8581977.
- [26] O. Tuna, Y. Selamet, G. Aygun, and L. Ozyuzer, "High quality ITO thin films grown by dc and RF sputtering without oxygen," *J. Phys. D. Appl. Phys.*, vol. 43, no. 5, 2010, doi: 10.1088/0022-3727/43/5/055402.
- [27] L. Wang, J. Wen, C. Yang, and B. Xiong, "Potential of ITO thin film for electrical probe memory applications," *Sci. Technol. Adv. Mater.*, vol. 19, no. 1, pp. 791–801, 2018, doi: 10.1080/14686996.2018.1534072.